
Article:
Walling, S.A., Notman, S., Watts, P. et al. (2019) Portland cement based immobilization/destruction of chemical weapon agent degradation products. Industrial & Engineering Chemistry Research, 58 (24). pp. 10383-10393. ISSN: 0888-5885

https://doi.org/10.1021/acs.iecr.9b01270

I&EC research
Industrial & Engineering Chemistry Research

Article

Cite This: Ind. Eng. Chem. Res. 2019, 58, 10383−10393

pubs.acs.org/IECR

Portland Cement Based Immobilization/Destruction of Chemical Weapon Agent Degradation Products

Sam A. Walling,[†] Stuart Notman,[‡] Pat Watts,[‡] Norman Govan,[‡] and John L. Provis*[,†]

[†]Immobilisation Science Laboratory, Department of Materials Science & Engineering, University of Sheffield, Sheffield, S1 3JD, United Kingdom

[‡]Defence Science and Technology Laboratory, Porton Down, Salisbury, SP4 0JQ, United Kingdom

ABSTRACT: The direct immobilization and destruction of two compounds relevant to chemical warfare agents, ethyl methylphosphonic acid (EMPA) and thiodiglycol (TDG), within a freshly mixed Portland cement paste was studied. Cement hydration and phase formation were analyzed to determine the upper limits on the loading of these chemicals achievable in an immobilization setting. EMPA, a degradation product of the nerve agent VX, alters the phase formation within the cements, allowing calcium aluminate dissolution while retarding hydration of calcium silicate clinker phases. This yielded ettringite, and sufficient calcium silicate hydrate for setting at 10 wt % loading, but the cohesive calcium silicate binding phase was lacking when EMPA was added at 25 wt %. The addition of TDG, a degradation product of sulfur mustard, uniformly retards the entire range of cement hydration mechanisms. Heat output was lowered and extended over a longer time frame, and less strength forming phases were produced. Up to 10% wt. TDG could be accommodated by the cement, but higher loadings caused severe disruption to the cement setting. This work demonstrates the ability of Portland cement to directly incorporate up to 10% wt. of these contaminants, and still form a stable set cement with conventional hydration phases.

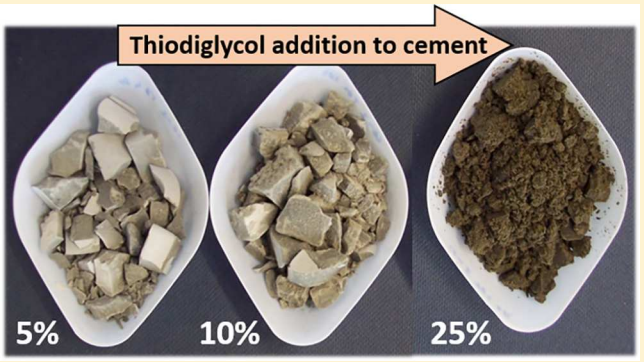

1. INTRODUCTION

The safe destruction and disposal of chemical warfare agents (CWAs) is a major concern, given their highly toxic nature. Typically CWA stockpiles are disposed via incineration, alkaline hydrolysis, supercritical water oxidation, or a combination of these methods.[1,2] These typically require the construction of facilities to which hazardous materials must be transported. This study aims to determine whether some of these agents might be disposed directly within a cement matrix. This could provide a field-deployable flexible system, which could operate on a small scale and be moved to wherever required, including potential operation under adverse environments.

Cements and grouts can be used to immobilize a wide range of hazardous materials. They are a mature technology for immobilization of toxic and radioactive wastes, with extensive usage for encapsulation of both liquid and solid waste streams over more than 50 years.[3,4] These wasteforms produce stable monoliths, maintain a high internal pH, are robust to waste variability, and can enable remote processing.[5,6]

Portland cement forms an alkaline slurry when mixed with water, initially due to dissolution of soluble alkali metal compounds from the cement clinker. This high pH is maintained via the hydration of cement clinker phases alite (Ca_3SiO_5) and belite (Ca_2SiO_4), which constitute 50−70% and 15−30% of the cement powder, respectively. These react with water to form a poorly crystalline hydrated calcium silicate mineral ("C−S−H") which is the main strength giving phase within Portland cements, with excess calcium precipitating as $Ca(OH)_2$, and the aluminate and calcium sulfate constituents of the cement also hydrate together to form complex calcium sulfoaluminate hydrates including ettringite and hydrocalumite-group ("AFm") phases.[7,8] The high pH and physical encapsulation routes offered by cements provide a unique opportunity for a flexible, low cost disposal system for CWAs.

There is an extensive body of scientific literature on CWA degradation on concrete surfaces, determining persistence and degradation mechanisms to understand their properties if they were to be deployed in the built environment, though little literature exists regarding the effects of CWAs or their degradation productions on the hydration and setting of cements. Nerve agents have been found to degrade quickly on concrete substrates, typically resulting in phosphonic acids which are neutralized by the alkaline concrete.[1,9] VX largely degrades to ethyl methylphosphonic acid (EMPA) (then to methylphosphonic acid (MPA)), along with various other minor components, within 1 day of concrete contact; fresh concrete causes faster degradation due to its higher basicity.[10−13]

Received: March 6, 2019
Revised: May 18, 2019
Accepted: May 29, 2019
Published: May 29, 2019

DOI: 10.1021/acs.iecr.9b01270
Ind. Eng. Chem. Res. 2019, 58, 10383−10393

Degradation in a basic environment has the additional benefit that it does not result in formation of VX-acids, such as the toxic EA-2192, which can occur during hydrolysis in water.[14]

G series nerve agents react rapidly in alkaline solutions to form nontoxic products, and bulk neutralization of such agents with NaOH is a tested and utilized destruction method.[1] At pH > 10, sarin (GB) and soman (GD) are hydrolyzed within a few minutes to MPA,[1,15] with tabun (GA) degrading to phosphoric acid. As the degradation products are acidic, this destruction needs an excess of base to reach complete destruction. Of the blister agents, mustard (HD) is the most studied, predominantly degrading via hydrolysis to thiodiglycol (TDG) and 1,4-oxathiane (along with minor vinyl species), with degradation quicker in fresh, wet concrete compared to aged concrete.[16−18] A half-life of up to 54 weeks was recorded for concrete in ambient conditions, compared to 2 weeks on moist concrete.[17] However, none of these studies have blended the CWAs directly into fresh cement during setting, which is the proposed disposal method investigated here.

This study looks at the effects of the VX degradation product EMPA, and the HD degradation product TDG, on the setting mechanisms and phase formation within Portland cement, to determine whether direct cement encapsulation and destruction of CWAs may be a viable prospect.

2. EXPERIMENTAL METHODOLOGY

Portland cement, CEM I 42.5N according to BS EN 206, was supplied by Hope Construction Materials, UK, with oxide composition as shown in Table 1. Portland cement pastes were mixed with increasing concentrations of 2,2′-thiodiethanol (thiodiglycol, TDG; > 99%, Sigma-Aldrich) and ethyl methylphosphonic acid (EMPA; > 98%, Dstl) to determine the effects of these CWA degradation products on cement hydration mechanisms. Distilled water was used in all mixes.

Table 1. Composition of CEM I, As Determined by X-ray Fluorescence Spectroscopy. LOI is Loss on Ignition at 1000°C

oxide	wt. %
CaO	63.86
SiO_2	19.81
Al_2O_3	5.33
SO_3	3.41
Fe_2O_3	2.49
MgO	0.98
Na_2O	0.92
K_2O	0.58
TiO_2	0.29
P_2O_5	0.24
LOI	1.27

The organics were added at 0, 5, 10, and 25% by total mass of all material, Table 2. Samples were prepared through addition of water to cement powder, followed by EMPA or TDG, before being gently stirred by hand to achieve full powder wetting, then mechanically mixed for 5 min at 1650 rpm using a Heidolph RZR 2020 overhead stirrer for 5 min at 1650 rpm in 150 mL pots, in large enough batches to enable homogeneous mixing. Samples were cast into either 15 mL centrifuge tubes or polymeric isothermal conduction calorimetry vials, and cured at 20 °C (except for those which were measured for calorimetry, which was conducted at 25 °C for 7 days in a TAM Air instrument). X-ray diffraction (XRD) and nuclear magnetic resonance (NMR) spectroscopic analysis were performed after 7 days of curing; samples were crushed, dried over NaOH in a vacuum desiccator to remove residual water, ground in an agate mortar, and passed through a 63 μm brass sieve. Samples were then sealed in airtight bags for analysis.

Table 2. Paste Formulations

cement powder (g)	EMPA or TDG (g)	H_2O (g)	water/cement mass ratio	wt % EMPA or TDG	liquid/solids mass ratio
20	0	7	0.35	0	0.35
20	1.4	7	0.35	5	0.4
20	3	7	0.35	10	0.5
20	9	7	0.35	25	0.8

Mixes were formulated at a constant water/cement mass ratio, to ensure availability of enough water for clinker hydration. This results in an increasing overall liquids/solids ratio as more organics are added.

X-ray diffraction was undertaken for random powder mounts using a PANalytical X'PERT^3 with Cu Kα radiation, 0.01313° step size, 0.36 s per step, collecting data between 5 and 70° 2θ. NMR spectroscopy was conducted using a Bruker AVIII spectrometer (9.4 T), using a 4 mm ^{1}H−^{19}F/X cross-polarization/magic angle spinning (CP/MAS) probe head, with samples packed into 4 mm o.d. zirconia rotors. ^{27}Al MAS spectra were collected at 104.212 MHz, spinning at 13 kHz, with a pulse duration of 0.8 μs (30°) and a recycle delay of 2 s, for an average of 1024 scans. Chemical shifts were referenced to 0.1 M $AlNO_3$. ^{13}C{^{1}H} high power decoupling (HPDEC) MAS spectra were collected at 100.573 MHz, spinning at 8 kHz, with a pulse duration of 4.0 μs (90°) and a recycle delay of 5 s, for an average of 2048 scans. ^{1}H decoupling was performed using the spinal64 pulse sequence[19] during acquisition at 100 kHz field strength. Chemical shifts were referenced to TMS. ^{29}Si MAS spectra were collected at 79.450 MHz, spinning at 4 kHz, with a pulse duration of 4.5 μs (45°) and a recycle delay of 240 s, for an average of 1024 scans. Chemical shifts were referenced to TMS. ^{31}P{^{1}H} HPDEC MAS spectra were collected at 161.899 MHz, spinning at 8 kHz, with a pulse duration of 4 μs (90°) and a recycle delay of 5 s, for an average of 512 scans. Chemical shifts were referenced to 85% wt. H_3PO_4.

XRF analysis of the Portland cement was undertaken on a PANalytical Zetium, using lithium borate beads made on a Claisse LeNeo Fluxer using 10.0003 g of lithium borate (Claisse anhydrous lithium tetraborate with lithium iodide (99.50% $Li_2B_4O_7$ − 0.50% LiI) and 1.0003 g Portland cement. This was poured into a 25 mL Pt crucible, mixed and fused into a 37 mm bead at 1065 °C for 22 min.

3. RESULTS AND DISCUSSION

3.1. EMPA. The addition of EMPA to the cement resulted in a vigorous immediate reaction, causing bubbling and releasing appreciable amounts of heat in the process. The reaction slowed after 3−4 min of stirring, and after this the paste exhibited rheology similar to that of a conventional Portland cement paste. The cements all solidified, successfully encapsulating up to 25 wt % loading of EMPA. The impact of EMPA on cement hydration is linked to how much alkalinity is consumed by EMPA neutralization to the salt form, and whether EMPA degrades to MPA. This would result in ethanol formation, which is known to arrest cement hydration.[20]

DOI: 10.1021/acs.iecr.9b01270
Ind. Eng. Chem. Res. 2019, 58, 10383−10393

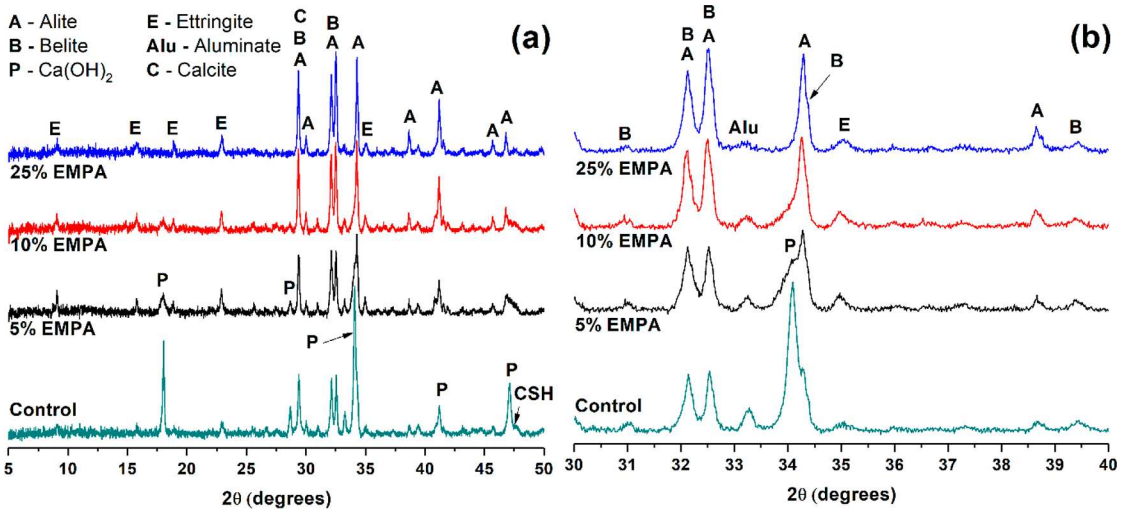

Figure 1. X-ray diffraction patterns of CEM I−EMPA mixes at 7 days of curing, showing (a) 5−50° pattern and (b) enlarged 30−40° section.

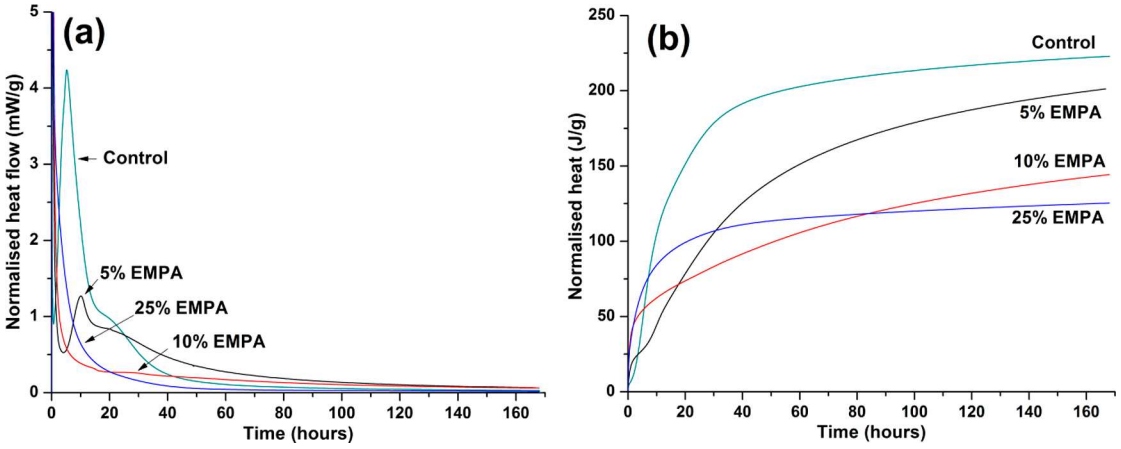

Figure 2. Isothermal calorimetry data for CEM I−EMPA mixes up to 168 h (7 days) of reaction. (a) Heat flow, (b) total heat evolution. All data are normalized to the mass of Portland cement in each mix.

Analysis of the hardened paste by X-ray diffraction, Figure 1, reveals a diffraction pattern typical of a hydrated Portland cement, exhibiting both unreacted clinker phases and the formation of hydrated binder phases. Unreacted alite (Ca_3SiO_5) (PDF no. 01−070−8632) and belite (Ca_2SiO_4) (PDF no. 01−086−0398) exhibit overlapping reflections at 29.4°, 32.1°, and 32.5° 2θ. However, the presence of both the minor alite reflection at 30.0°, and the minor belite reflection at 30.9°, is the best indicator that both of these clinker phases still remain in the hardened paste. The principal tricalcium aluminate ("aluminate", $Ca_3Al_2O_6$) (PDF no. 01−070−0839) reflection is at 33.2°, while the principal calcium aluminoferrite ("ferrite", $Ca_2(Al,Fe)_2O_5$) (PDF no. 01−071−0667) reflection occurs at 33.9°, directly underneath a major reflection of the hydration product portlandite ($Ca(OH)_2$) (PDF no. 01−072−0156). Typically ferrite can also be identified by a secondary reflection at 12.2°, although this is not identifiable in any of the diffractograms here. $Ca(OH)_2$ is additionally identifiable by clear peaks at 18.0° and 47.1° 2θ, indicating substantial alite and/or belite hydration.

The principal strength-giving phase within hydrated Portland cements is a poorly crystalline hydrated calcium silicate phase, denoted "C−S−H", which develops through hydration of alite and belite, with minor Al substitution occurring. Typically this phase exhibits a diffuse reflection around 28° 2θ, which is very broad and directly overlaps $Ca(OH)_2$ and calcite (PDF no. 01−086−0174) reflections, making its identification here difficult. A secondary reflection can often be observed between 46.5° to 48°, though this is partially obscured by another $Ca(OH)_2$ reflection, and a minor alite reflection. This diffuse band can be more easily seen in the 5 wt % EMPA diffraction pattern in Figure 1(a). Ettringite ($Ca_6Al_2(SO_4)_3(OH)_{12}\cdot 26H_2O$) (PDF no. 00−041−1451) is also present throughout the diffractions, due to aluminate/ferrite reaction with the interground gypsum. There is also likely to be some calcium monosulfoaluminate hydrate ("monosulfate", $Ca_4Al_2(SO_4)(OH)_{12}\cdot 6H_2O$) (e.g., PDF no. 01−083−1289), although in quantities too small, and/or with crystallinity too low, to be easily visible by XRD. The phases observed are typical for conventional Portland cement pastes.[7,21]

Addition of EMPA into the CEM I mix affects $Ca(OH)_2$ formation; the reflections associated with this phase drop substantially in intensity, while those associated with ettringite increase slightly. This is broadly consistent with higher intensity of the peaks due to residual alite and belite, suggesting decreased reaction of these phases, especially in the 10 and 25 wt %. EMPA samples. This correlates with a decrease in the C−S−H reflection around 47° 2θ. Although alite and belite appear

DOI: 10.1021/acs.iecr.9b01270
Ind. Eng. Chem. Res. 2019, 58, 10383−10393

inhibited, addition of EMPA appears to allow, or even accelerate, aluminate (and presumably ferrite) hydration, with resulting ettringite formation.

Isothermal calorimetry provides a further tool to identify phase formation within the cements, and particularly whether clinker hydration is suppressed. The data obtained are shown in Figure 2, with the control sample displaying a typical cement calorimetry curve.[22,23] This consists of rapid initial reaction within 1 h with dissolution of alite and aluminate, and rapid precipitation of ettringite within a few minutes. Alite dissolution and ettringite precipitation then continue at a lower level; the products of the alite dissolution reach supersaturation and precipite a C−S−H gel and $Ca(OH)_2$. This peaks at ∼8 h and begins to decelerate, before a second shoulder ∼15 h into hydration can be seen, which is likely formation of the monosulfate phase as sulfate depletion destabilizes ettringite. Both of these reactions slow down, largely leveling off after 40 h. After this period unreacted alite continues to slowly react, along with a slow reaction of belite and ferrite over the next few days to months.[22,23]

The addition of EMPA severely affects the cement hydration. With 5 wt % addition there is a high initial heat output due to ettringite formation and the heat of neutralization of the EMPA. Following this a recognizable cement hydration occurs; however, it is retarded, producing a lower heat output, and extended over a longer time frame. Total heat output (Figure 2b) is not far behind the control cement after 160 h, suggesting hydration and formation of a C−S−H gel, but over a longer period. The addition of 10 and 25 wt % EMPA results in a high early heat output and little (or slow) later reaction of clinker. No characteristic hydration peaks were observed, and there is a notable decrease in overall heat output, suggesting suppression of alite/belite hydration, especially in the 25 wt % EMPA sample. Phosphonates are known to suppress and retard cement hydration, including via calcium complexation as well as the formation of layered calcium phosphonates that can mask the surfaces of clinker grains and hinder their reaction.[24]

After the sample vials were removed from the calorimeter, the cement was extracted from the vials for physical examination, Figure 3. All samples had set solid, with no bleed liquid

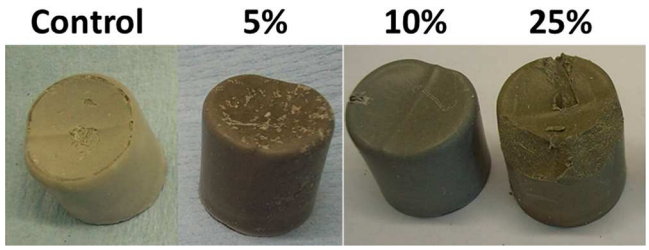

Figure 3. Photographs of CEM I−EMPA mixes after removal from calorimeter. Diameter of each sample is approximately 24 mm.

observable. Aside from imparting a darker color to the samples, addition of 5 and 10 wt % EMPA did not appear to affect the physical characteristics. With 25 wt % EMPA loading the sample was solid, but it deformed when struck with a hammer, and bounced slightly if dropped. The ability of this sample to remain solid is surprising considering the lack of appreciable C−S−H gel formation observed in the XRD and calorimetric data. This could be due to large quantities of ettringite, or perhaps formation of a poorly crystalline aluminophosphate gel; these possibilities will be investigated below.

Further detailed analysis of the interactions between EMPA/TDG and the cement paste can be undertaken by solid state NMR spectroscopy. This first requires detailed analysis of the control cement, Figures 4 and 5. Figure 4a displays the ^{29}Si NMR spectrum of the control CEM I sample, with suggested subpeaks plotted underneath. Subpeaks were plotted using Gaussian distributions positioned according to known Si sites in cements. Both alite and belite are present within the spectrum, tallying with the unreacted clinker observed in XRD analysis. The deconvolution for belite follows the spectrum of β-Ca_2SiO_4, while the alite has been simplified from its highly complex line shape to two broadened Gaussian peaks, reflecting impurities in the pure tricalcium silicate structure.[25,26] The resonance of the C−S−H phase in this sample is upfield of the alite and belite, typically partially Al substituted to make a C−(A−)S−H phase, with characteristic peaks in the region −75 to −100 ppm.

Deconvolution of the spectrum of C−S−H was based on literature for Portland cements and model C−(A−)S−H gels, consisting of primarily end group Q^1 and chain Q^2 SiO_4 units,[27,28] with Al incorporated in bridging sites between SiO_4 tetrahedra, forming $Q^2(1Al)$ species.[27] Data shown here are typical for this age, showing that a developed C−(A−)S−H network has formed, while some quantity of silicate clinker phases remain unreacted.

The ^{27}Al MAS NMR spectrum of the hydrated control cement is detailed in Figure 4b, with a clear separation between the Al(IV) and Al(VI) regions. The Al(IV) region contains aluminum associated with unreacted clinker phases and in bridging sites within the C−(A−)S−-H gel. Both alite and belite add to the signal at ∼80−85 ppm due to Al incorporation in these silicate phases during clinker production.[25−27] Alite is limited to ∼1% Al_2O_3 incorporation, with belite typically 4−6%.[21] The aluminate and ferrite phases contribute throughout this spectrum. Aluminate produces a complex broad signal between 70 and 0 ppm, and ferrite produces a peak at ∼13 ppm, although broadened and suppressed due to the presence of iron in this phase.

The Al(VI) region contains aluminum within ettringite, monosulfate, and a third aluminate hydrate (TAH) phases. Both aluminate and ferrite react with $CaSO_4$, forming ettringite and monosulfate,[8,29] identified in the Al(VI) region at 14.7 and 11.5 ppm, respectively. There is also a small contribution from a third aluminate hydrate phase upfield of monosulfate; this is believed to be an aluminate sorbed on other cement constituents.[27]

The analysis of Portland cement with $^{31}P\{^1H\}$ HPDEC NMR was utilized to enable the study of EMPA interactions. Portland cement contains little phosphorus; P_2O_5 from raw materials or kiln fuels can enter alite and belite, with PO_4^{3-} units substituting for SiO_4^{4-} tetrahedra. This is typically <0.5% by mass of cement,[30−32] with 0.24% here (Table 1), limiting the signal-to-noise ratio achieved. The single peak in the $^{31}P\{^1H\}$ spectrum is shown in Figure 5a, at ∼3.4 ppm. This most likely corresponds to P incorporating into interlayers of C−(A−)S−H.[30]

^{13}C NMR spectroscopy is not a typical analytical method used for cements; however, due to the addition of organics (EMPA/TDG) into these cements, this should provide some information about their fate after hydration. Another HPDEC experiment was selected for this nucleus, looking at $^{13}C\{^1H\}$. The spectrum shown in Figure 5b exhibits a low signal-to-noise ratio with one primary peak with a broader base. This peak is attributed to calcite ($CaCO_3$) added as a minor cement constituent.

The incorporation of EMPA into cement has a notable effect on the NMR spectra. NMR analysis was undertaken on samples

DOI: 10.1021/acs.iecr.9b01270
Ind. Eng. Chem. Res. 2019, 58, 10383−10393

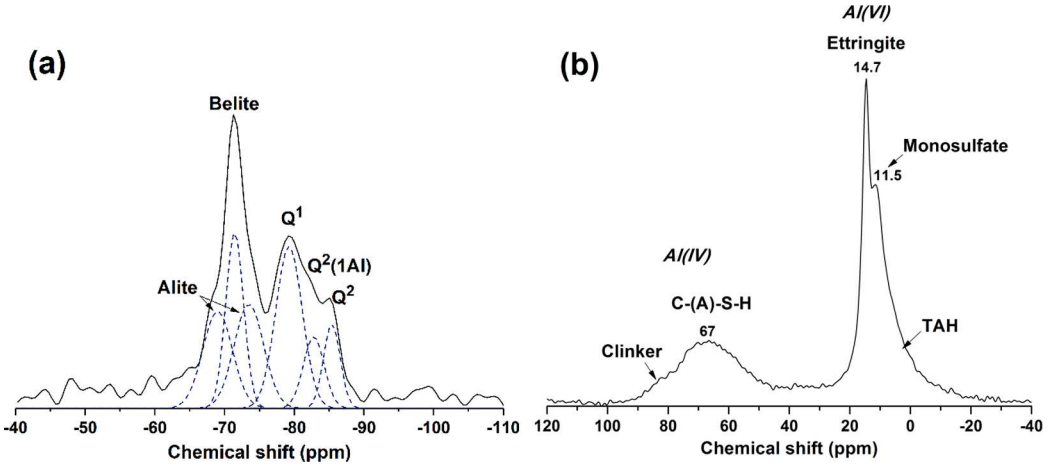

Figure 4. (a) ^{29}Si and (b) ^{27}Al MAS NMR spectra for CEM I at 7 days of curing. Suggested deconvolution peaks are plotted underneath the ^{29}Si spectrum.

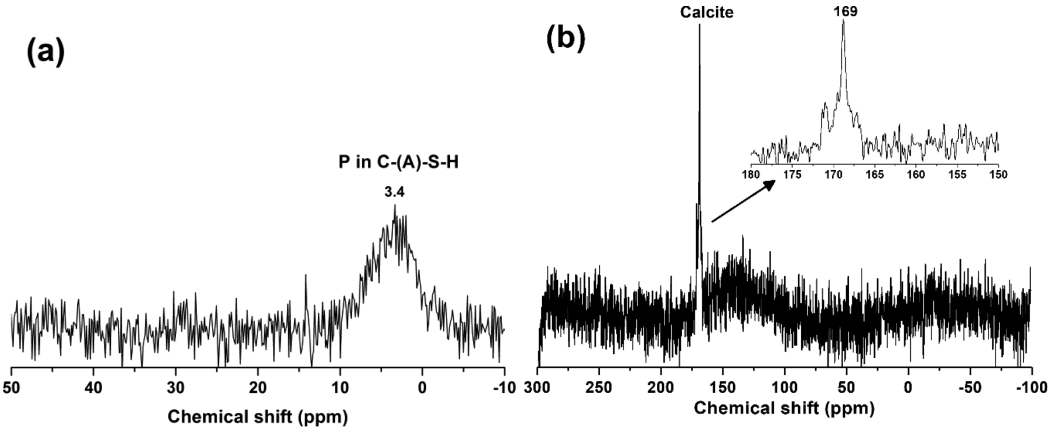

Figure 5. (a) ^{31}P{^{1}H} and (b) ^{13}C{^{1}H} HPDEC MAS NMR spectra for CEM I at 7 days of curing.

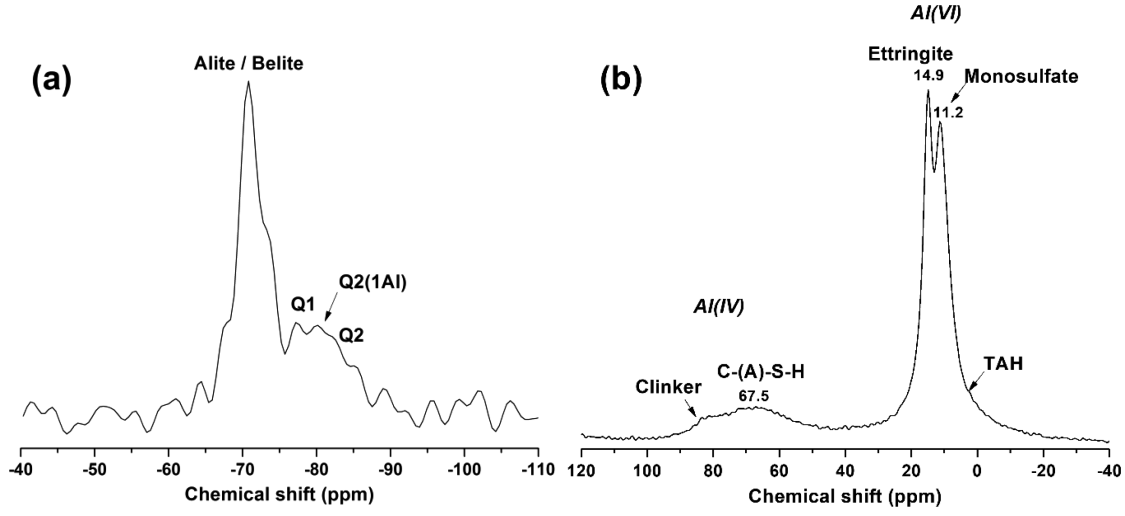

Figure 6. (a) ^{29}Si and (b) ^{27}Al MAS NMR spectra for the CEM I−5 wt % EMPA mix at 7 days of curing.

with 5 and 25 wt % EMPA, and the ^{29}Si and ^{27}Al MAS NMR spectra for 5 wt %. EMPA are shown in Figure 6. Significant quantities of alite and belite remain, and the C−(A−)S−H sites (Q^1, Q^2(1Al), and Q^2) have decreased in intensity compared to the control, indicating reduced formation of this gel. Correspondingly, the broad signal for C−(A−)S−H in the ^{27}Al spectrum appears reduced, and the strong signals for ettringite and monosulfate appear increased, commensurate with XRD results. There also remains again the potential for a third aluminate hydrate to exist slightly upfield; however, this is obscured by monosulfate if it is present.

With the addition of 5 wt % EMPA, there are additional resonances visible in the ^{31}P{^{1}H} and ^{13}C{^{1}H} NMR spectra in Figure 7 that were not seen in Figure 5 for the control. In the

DOI: 10.1021/acs.iecr.9b01270
Ind. Eng. Chem. Res. 2019, 58, 10383−10393

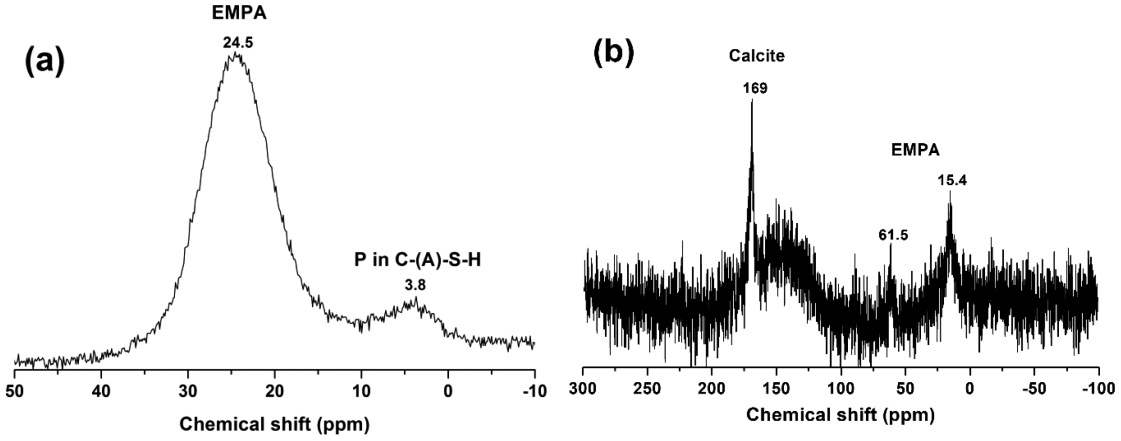

Figure 7. (a) $^{31}P\{^{1}H\}$ and (b) $^{13}C\{^{1}H\}$ HPDEC MAS NMR spectra for the CEM I−5% EMPA mix at 7 days of curing.

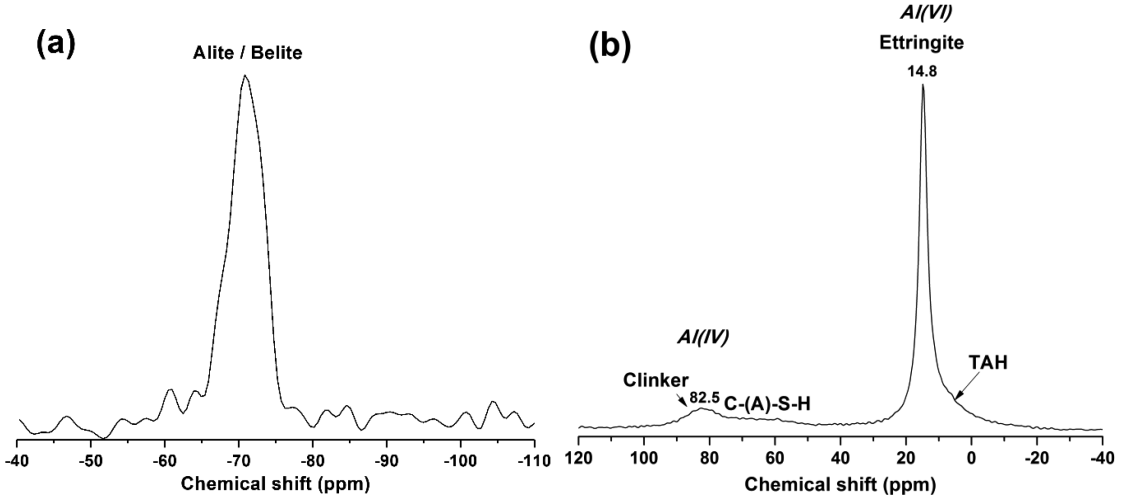

Figure 8. (a) ^{29}Si and (b) ^{27}Al MAS NMR spectra for the CEM I−25 wt % EMPA mix at 7 days of curing.

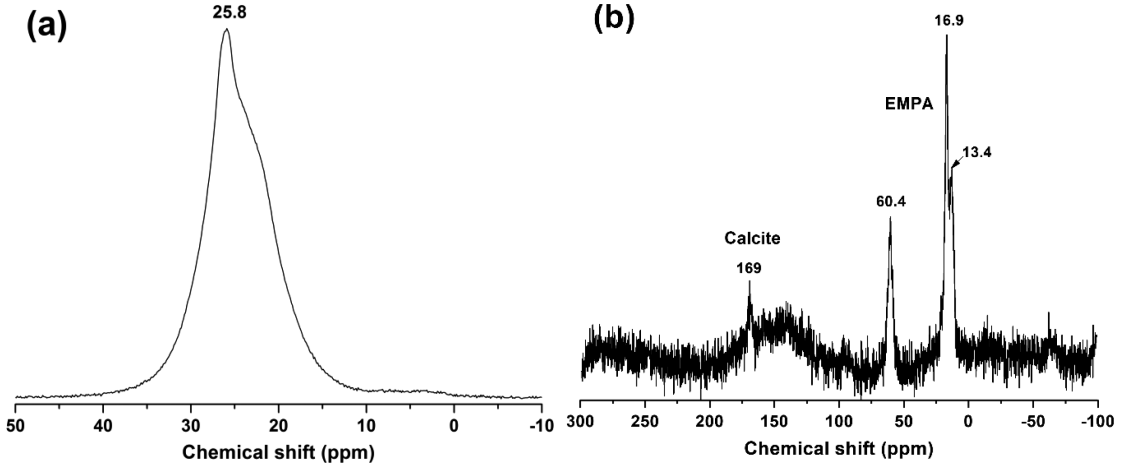

Figure 9. (a) $^{31}P\{^{1}H\}$ and (b) $^{13}C\{^{1}H\}$ HPDEC MAS NMR spectra for the CEM I−25 wt % EMPA mix at 7 days of curing.

$^{31}P\{^{1}H\}$ spectrum there remains the signal at ∼3.8 ppm due to interlayer P in C−(A−)S−H, however a much larger broad signal is seen at ∼24.5 ppm. This has been assigned to EMPA based on literature data, although this does not preclude MPA due to the broad nature of the resonance.[33,34] The $^{13}C\{^{1}H\}$ spectrum again shows the $CaCO_3$ peak at 172 ppm, however two new peaks appear at 61.5 and 15.4 ppm. These correlate well to the O-ethyl and PCH_3 groups of EMPA, and could also represent PCH_3 within MPA.[35]

With the addition of 25 wt % EMPA (Figure 8), the spectra display a significant change compared to the control and 5 wt % EMPA samples. The ^{29}Si MAS NMR spectrum does not show the presence of any sites associated with a C−(A−)S−H gel, with only alite and belite visible. No other Si sites are present,

DOI: 10.1021/acs.iecr.9b01270
Ind. Eng. Chem. Res. 2019, 58, 10383−10393

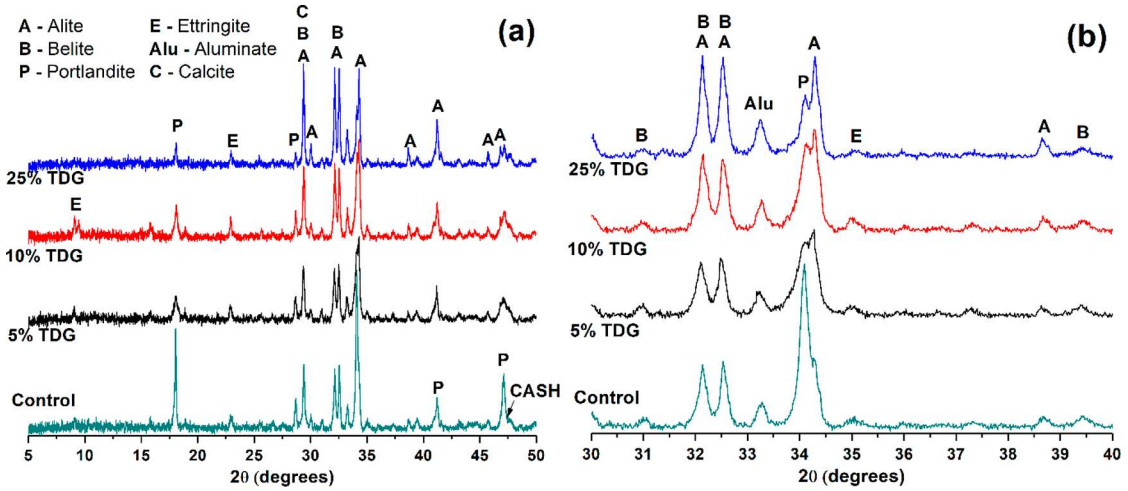

Figure 10. X-ray diffraction patterns of CEM I−TDG mixes at 7 days of curing.

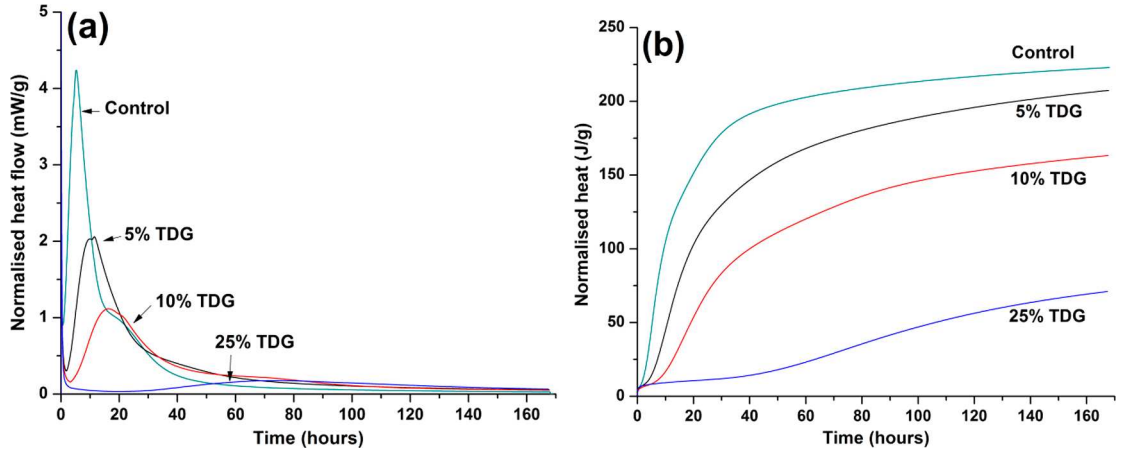

Figure 11. Isothermal calorimetry of CEM I−TDG mixes up to 168 h (7 days) of reaction. (a) Heat flow, (b) total heat evolution. All data are normalized to the mass of cement in each mix.

indicating that dissolution of alite and belite is suppressed, and that the formation of a phospho-silicate gel via reaction of the added EMPA is unlikely. However, because of the limited signal-to-noise ratio achieved (due to the long collection times required for ^{29}Si NMR spectra and the influence of iron in the cement) this result cannot fully preclude the formation of small amounts of C−(A−)S−H or other silicate environments.

Collection of ^{27}Al data is much faster, giving a better resolved signal. From Figure 8b it can be seen that a C−(A−)S−H gel might have formed, but at a much reduced level compared to the control or 5 wt % EMPA samples. The distinct peak from Al incorporated in alite and belite can be identified. A very strong signal attributed to ettringite is present within the Al(VI) region, in agreement with XRD analysis of this cement, and there is a small TAH resonance. Most notable is the lack of any other Al environments. The solid nature of the 25% EMPA sample, but without formation of significant C−(A−)S−H gel, led to postulation of an aluminophosphate gel formed from interaction between reacted aluminate/ferrite and the EMPA during neutralization. However, no Al environments consistent with such a phase have been identified in this spectrum, so the hypothesis must be discarded.

The incorporation of 25% EMPA further alters the ^{31}P{^{1}H} and ^{13}C{^{1}H} NMR spectra, Figure 9. The principal EMPA peak at ∼25 ppm has increased in intensity, and exhibits a shoulder upfield. This is typical of EMPA, but also overlaps with that of MPA.[36−39] The asymmetric peak suggests two P environments, potentially due to the presence of MPA. It seems unlikely that other phosphate minerals have been formed during EMPA neutralization. No other phosphates were identified with XRD analysis, and no other P environments can be identified here. Solid calcium phosphates such as $Ca_{10}(OH)_2(PO_4)$, $CaHPO_4$ or $Ca(H_2PO_4)_2{\cdot}H_2O$ typically exhibit ^{31}P resonances in the region 3 to −5 ppm.[40] Aluminophosphate resonances could range from 5 to −50 ppm,[41] a region in which no peaks were identified here (the data have been truncated at −10 ppm for plotting, but no peaks were identified during processing). The ^{13}C{^{1}H} NMR spectrum in Figure 9(b) shows an increased intensity and sharpness in the peaks at ∼60−61 and ∼15 ppm, with the latter revealing two peaks. Again these are assigned to ethyl and methyl groups in EMPA/MPA respectively, with no other carbon environments noted.

3.2. TDG. The TDG added into the cement samples reacted very differently from EMPA. In general the TDG mixed into samples well, and appears to uniformly depress cement hydration in line increasing dosage. The usual cement hydration products were observed by XRD in Figure 10, exhibiting lower intensity reflections for key cement hydrate phases with increasing TDG concentration. Compared to addition of EMPA, there are stronger reflections for $Ca(OH)_2$ and a

DOI: 10.1021/acs.iecr.9b01270
Ind. Eng. Chem. Res. 2019, 58, 10383−10393

noticeable diffuse peak for C−(A−)S−H at ∼47° 2θ. Reflections for ettringite are lower, and the reflections for the residual aluminate phase are stronger, indicating less reaction of this cement constituent.

Calorimetric analysis of the TDG-containing samples, Figure 11, also shows uniform depression of cement hydration with increasing TDG concentration. This leads to reduced heat flow and a delay in the onset of hydration, resulting in a reduced total heat output. The addition of 25% TDG severely retards the system. Very little heat flow is detected for 30 h in this case, and then a very slow, low heat of hydration begins and continues until the cessation of the experiment. This suggests that up to 10% TDG might be the upper limit for incorporation within a CEM I system.

Removal of the samples from the calorimeter vials (Figure 12) reveals that the addition of 5 and 10 wt % TDG results in the formation of stable cement samples. Both were solid, with no bleed liquid observed. Conversely, the addition of 25 wt % TDG gave a dark, weak sample, which crumbled upon application of slight pressure. This was accompanied by a small quantity of bleed liquid.

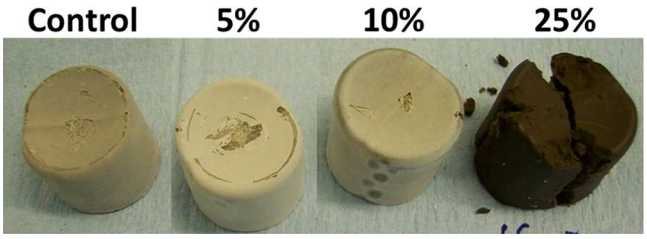

Figure 12. Photographs of CEM I−EMPA mixes after removal from calorimeter. Diameter of each sample is approximately 24 mm.

The results of this analysis indicate that TDG suppresses cement clinker hydration in proportion to TDG loading. The extreme suppression caused by the addition of 25% TDG results in a corresponding lack of strength forming phases, and thus a mechanically weak sample.

The ^{29}Si and ^{27}Al MAS NMR spectra for 5 wt % TDG addition into CEM I are shown in Figure 13. The resulting spectra are very similar to those for 5 wt % addition of EMPA, with resonances of unreacted alite and belite, along with a C−(A−)S−H gel, constituting the ^{29}Si MAS NMR spectrum. The ^{27}Al MAS NMR spectrum again shows tetrahedral Al within a C−(A−)S−H gel, unreacted clinker, ettringite, monosulfate, and possible contributions from TAH. No additional environments have been identified, in line with XRD analysis suggesting overall suppression of hydration but no major changes in reaction pathways or products.

Increasing the incorporation of TDG up to 25 wt % continues to alter the composition of the cement paste. This can be seen in the ^{29}Si MAS NMR spectrum, Figure 14a, where only low intensity signals are present within the C−(A−)S−H region around −75 to −90 ppm, revealing only minor formation of this gel and weak alite/belite dissolution. The ^{27}Al MAS NMR spectrum in Figure 14b continues this trend, revealing unreacted clinker at ∼81.2 ppm, with a low but observable shoulder for C−(A−)S−H along with a signal for ettringite.

The ^{31}P{^{1}H} spectra for 5% TDG incorporation (Figure 15a) shows typical incorporation of P within C−(A−)S−H interlayers, as identified for the control (Figure 5). As TDG adds no extra phosphorus into the system, this is as expected. ^{13}C{^{1}H} NMR (Figure 15b) once again reveals $CaCO_3$ at ∼169 ppm, and two new peaks at 62.1 and 35.1 ppm assigned to TDG.[42]

Increasing the level of TDG to 25%, Figure 16, hydrated phosphorus is again only present within the interlayer of the C−(A−)S−H gel. The ^{13}C{^{1}H} HPDEC spectrum again reveals the calcite peak at ∼169 ppm, along with two strong signals for TDG at 62.3 and 35.2 ppm.[33,42] No other degradation or breakdown products have been detected.

The solid state NMR data detailed here for TDG reveal the overall suppression of Portland cement clinker hydration in a fairly uniform fashion. C−(A−)S−H and ettringite are formed, although in apparently lesser amounts than in the control sample, or with only 5 wt % TDG addition. The TDG appears to remain relatively unreacted and does not produce any other breakdown products.

4. CONCLUSIONS

EMPA and TDG both affect the setting and hydration phase assemblages within Portland cements, though both are able to be incorporated up to 10% by weight without severely compromising the structural and chemical integrity of a cement wasteform.

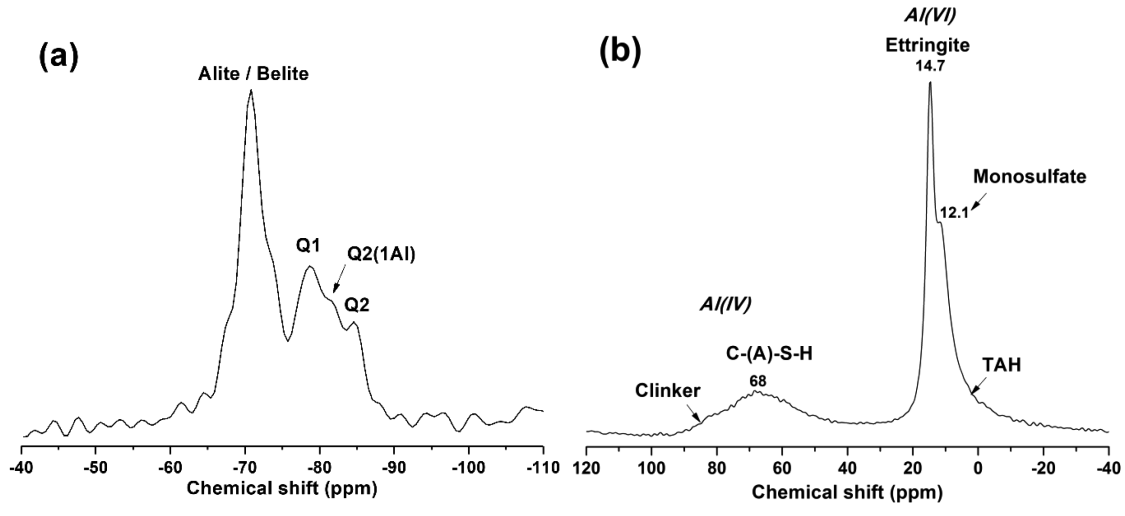

Figure 13. (a) ^{29}Si and (b) ^{27}Al MAS NMR spectra for the CEM I−5% TDG mix at 7 days of curing.

DOI: 10.1021/acs.iecr.9b01270
Ind. Eng. Chem. Res. 2019, 58, 10383−10393

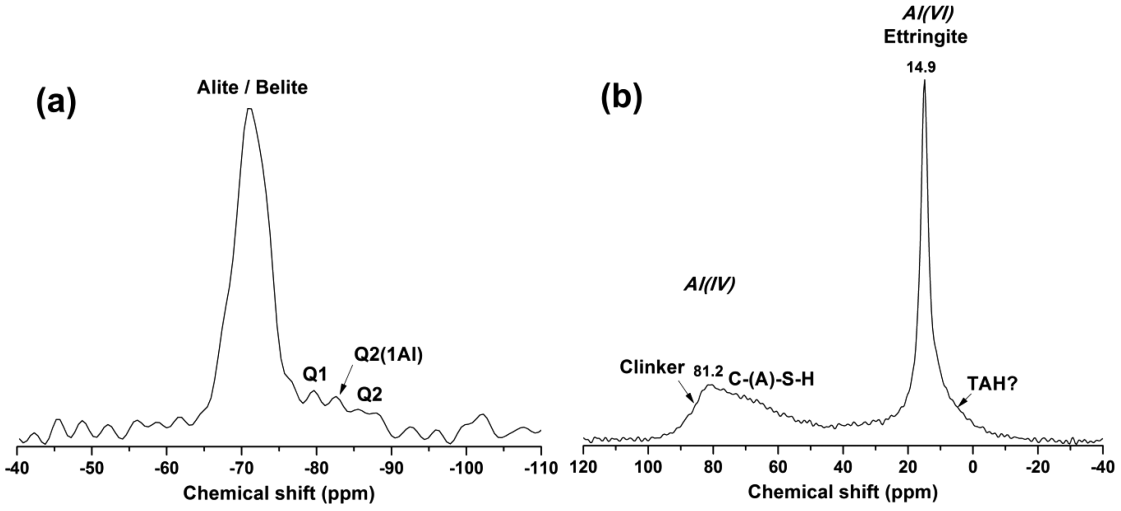

Figure 14. (a) ^{29}Si and (b) ^{27}Al MAS NMR spectra for the CEM I−25 wt % TDG mix at 7 days of curing.

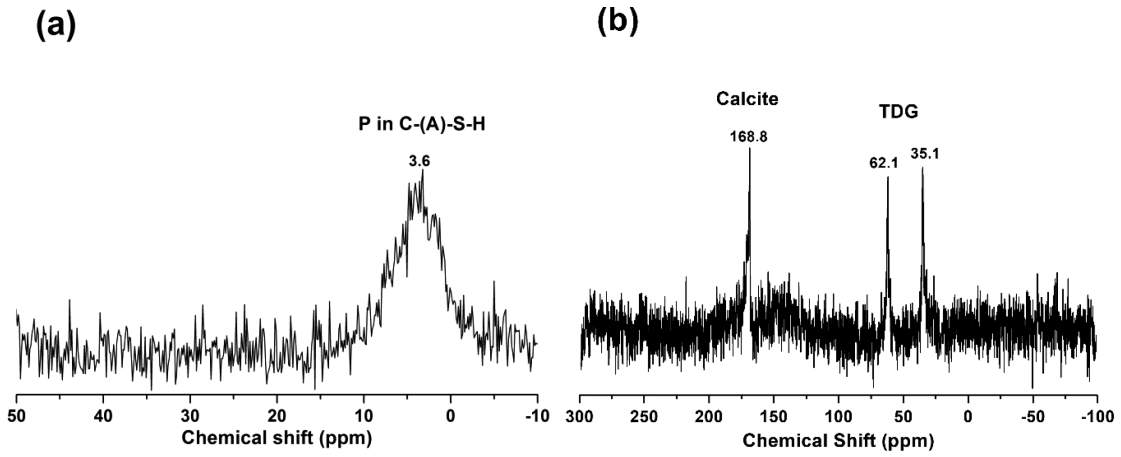

Figure 15. (a) ^{31}P{^{1}H} and (b) ^{13}C{^{1}H} HPDEC MAS NMR spectra for the CEM I−5 wt % TDG mix at 7 days of curing.

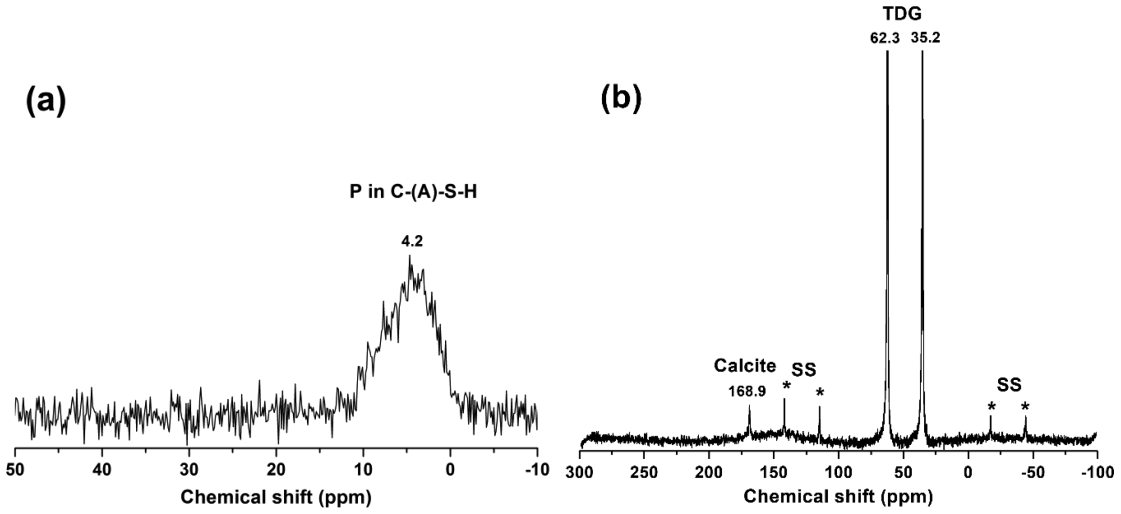

Figure 16. (a) ^{31}P{^{1}H} and (b) ^{13}C{^{1}H} HPDEC MAS NMR spectra for CEM I−25% TDG mix at 7 days of curing. Peaks marked with * are spinning sidebands of the principal resonances.

EMPA reacts with the cement paste exothermically, suppressing C−(A−)−S−H formation, while allowing calcium aluminate phases to form. This enables a solid structure to form even at 25% waste loading. TDG appears to uniformly suppress cement clinker hydration, reducing and slowing heat output and hydrated phase formation. At the highest TDG loading, this results in few hydration products and a failure to set. If cementitious systems were to be utilized for CWA destruction,

DOI: 10.1021/acs.iecr.9b01270
Ind. Eng. Chem. Res. 2019, 58, 10383−10393

these degradation products are likely to be tolerated by the cements before setting occurs, unless produced in very high quantities. However, the data herein cannot be extrapolated to the neat nerve or blister agents, and for evaluation of their susceptibility to immobilization by cementation, the corresponding experiments would need to be performed with the toxic compounds themselves. The interaction of these materials with a cementitious system should also be further studied over a longer time frame to determine any further clinker reactions, combined with leach testing to assess the disposability of any wasteforms produced.

AUTHOR INFORMATION

Corresponding Author

*Phone +44 114 222 5490; e-mail j.provis@sheffield.ac.uk.

ORCID

John L. Provis: 0000-0003-3372-8922

Notes

The authors declare no competing financial interest.

ACKNOWLEDGMENTS

This research was funded by Dstl and performed in part at the MIDAS Facility, at the University of Sheffield, which was established with support from the Department of Energy and Climate Change. We thank Dstl for sharing extensive technical expertise, especially Dr. James Jones for NMR acquisition.

REFERENCES

(1) Jang, Y. J.; Kim, K.; Tsay, O. G.; Atwood, D. A.; Churchill, D. G. Update 1 of: Destruction and detection of chemical warfare agents. *Chem. Rev.* **2015**, *115*, PR1−PR76.

(2) Pearson, G. S.; Magee, R. S. Critical evaluation of proven chemical weapon destruction technologies (IUPAC technical report). *Pure Appl. Chem.* **2002**, *74*, 187−316.

(3) Glasser, F. P. Mineralogical aspects of cement in radioactive waste disposal. *Mineral. Mag.* **2001**, *65*, 621−633.

(4) Malviya, R.; Chaudhary, R. Factors affecting hazardous waste solidification/stabilization: A review. *J. Hazard. Mater.* **2006**, *137*, 267−276.

(5) Ojovan, M.I.; Lee, W.E. *An Introduction to Nuclear Waste Immobilisation*; Elsevier: Oxford, 2005.

(6) Sharp, J. H.; Hill, J.; Milestone, N. B.; Miller, E. W. Cementitious systems for encapsualation of intermediate level waste. *ASME Conference Proceedings* **2003**, *2003*, 1425−1433.

(7) Lothenbach, B.; Le Saout, G.; Gallucci, E.; Scrivener, K. Influence of limestone on the hydration of Portland cements. *Cem. Concr. Res.* **2008**, *38*, 848−860.

(8) Lothenbach, B.; Winnefeld, F. Thermodynamic modelling of the hydration of Portland cement. *Cem. Concr. Res.* **2006**, *36*, 209−226.

(9) Munro, N. B.; Talmage, S. S.; Griffin, G. D.; Waters, L. C.; Watson, A. P.; King, J. F.; Hauschild, V. The source, fate, and toxicity of chemical warfare agent degradation products. *Environ. Health Perspect.* **1999**, *107*, 933−974.

(10) Creasy, W. R.; McGarvey, D. J.; Brevett, C. A. S. Speciation of VX in aqueous solutions. *J. Phys. Chem. C* **2013**, *117*, 22677−22682.

(11) Groenewold, G. S.; Appelhans, A. D.; Gresham, G. L.; Olson, J. E.; Jeffery, M.; Weibel, M. Characterization of VX on concrete using ion trap secondary ionization mass spectrometry. *J. Am. Soc. Mass Spectrom.* **2000**, *11*, 69−77.

(12) Columbus, I.; Waysbort, D.; Marcovitch, I.; Yehezkel, L.; Mizrahi, D. M. VX fate on common matrices: evaporation versus degradation. *Environ. Sci. Technol.* **2012**, *46*, 3921−3927.

(13) Wagner, G. W.; O'Connor, R. J.; Edwards, J. L.; Brevett, C. A. S. Effect of drop size on the degradation of VX in concrete. *Langmuir* **2004**, *20*, 7146−7150.

(14) Wagner, G. W.; O'Connor, R. J.; Procell, L. R. Preliminary study on the fate of VX in concrete. *Langmuir* **2001**, *17*, 4336−4341.

(15) Yang, Y.-C.; Baker, J. A.; Ward, J. R. Decontamination of chemical warfare agents. *Chem. Rev.* **1992**, *92*, 1729−1743.

(16) Brevett, C.A.S.; Nickol, R.G.; Sumpter, K.B.; Wagner, G.W. *Degradation of the Blister Agent Bis(2-chloroethyl) Sulfide and Simulant 2-Chloroethyl Phenyl Sulfide on Concrete*; Edgewood Chemical Biological Center: Aberdeen Proving Ground, MD, 2007.

(17) Brevett, C. A. S.; Sumpter, K. B.; Nickol, R. G. Kinetics of the degradation of sulfur mustard on ambient and moist concrete. *J. Hazard. Mater.* **2009**, *162*, 281−291.

(18) Mizrahi, D. M.; Goldvaser, M.; Columbus, I. Long-term evaluation of the fate of sulfur mustard on dry and humid soils, asphalt, and concrete. *Environ. Sci. Technol.* **2011**, *45*, 3466−3472.

(19) Fung, B. M.; Khitrin, A. K.; Ermolaev, K. An improved broadband decoupling sequence for liquid crystals and solids. *J. Magn. Reson.* **2000**, *142*, 97−101.

(20) Zhang, J.; Scherer, G. W. Comparison of methods for arresting hydration of cement. *Cem. Concr. Res.* **2011**, *41*, 1024−1036.

(21) Taylor, H. F. W. *Cement Chemistry*, 2nd ed.; Thomas Telford Publishing: London, UK, 1997.

(22) Bullard, J. W.; Jennings, H. M.; Livingston, R. A.; Nonat, A.; Scherer, G. W.; Schweitzer, J. S.; Scrivener, K. L.; Thomas, J. J. Mechanisms of cement hydration. *Cem. Concr. Res.* **2011**, *41*, 1208−1223.

(23) Scrivener, K. L.; Juilland, P.; Monteiro, P. J. M. Advances in understanding hydration of Portland cement. *Cem. Concr. Res.* **2015**, *78A*, 38−56.

(24) Bishop, M.; Bott, S. G.; Barron, A. R. A new mechanism for cement hydration inhibition: Solid-state chemistry of calcium nitrilotris(methylene)triphosphonate. *Chem. Mater.* **2003**, *15*, 3074−3088.

(25) Skibsted, J.; Hall, C.; Jakobsen, H.J., Nuclear magnetic resonance spectroscopy and magnetic resonance imaging of cements and cement-based materials. In *Structure and performance of cements*; Bensted, J.; Barnes, P., Eds.; Spon Press: London, 2002; pp 457−476.

(26) Raupp-Pereira, F.; Segadães, A. M.; Silva, A. S.; Rocha, J.; Labrincha, J. A. ^{27}Al and ^{29}Si NMR and XRD characterisation of clinkers: standard phases and new waste based formulations. *Adv. Appl. Ceram.* **2008**, *107*, 37−45.

(27) Andersen, M. D.; Jakobsen, H. J.; Skibsted, J. Incorporation of aluminum in the calcium silicate hydrate (C-S-H) of hydrated Portland cements: A high-field ^{27}Al and ^{29}Si MAS NMR investigation. *Inorg. Chem.* **2003**, *42*, 2280−2287.

(28) Myers, R. J.; Bernal, S. A.; San Nicolas, R.; Provis, J. L. Generalized structural description of calcium−sodium aluminosilicate hydrate gels: the cross-linked substituted tobermorite model. *Langmuir* **2013**, *29*, 5294−5306.

(29) Odler, I., Hydration, setting and hardening of Portland cement. In *Lea's Chemistry of Cement and Concrete*; Hewlett, P.C., Ed.; Butterworth Heinemann: Oxford, UK, 2003; pp 241−297.

(30) Poulsen, S. L.; Jakobsen, H. J.; Skibsted, J. Incorporation of phosphorous guest ions in the calcium silicate phases of Portland cement from ^{31}P MAS NMR spectroscopy. *Inorg. Chem.* **2010**, *49*, 5522−5529.

(31) Macphee, D.E.; Lachowski, E.E., Cement components and their phase relations. In *Lea's Chemistry of Cement and Concrete*; Hewlett, P.C., Ed.; Butterworth Heinemann: Oxford, UK, 2003; pp 95−129.

(32) Poulsen, S. L.; Kocaba, V.; Le Saoût, G.; Jakobsen, H. J.; Scrivener, K. L.; Skibsted, J. Improved quantification of alite and belite in anhydrous Portland cements by ^{29}Si MAS NMR: Effects of paramagnetic ions. *Solid State Nucl. Magn. Reson.* **2009**, *36*, 32−44.

(33) Wagner, G. W.; Koper, O. B.; Lucas, E.; Decker, S.; Klabunde, K. J. Reactions of VX, GD, and HD with nanosize CaO: autocatalytic dehydrohalogenation of HD. *J. Phys. Chem. B* **2000**, *104*, 5118−5123.

(34) Brevett, C. A. S.; Sumpter, K. B.; Pence, J.; Nickol, R. G.; King, B. E.; Ginannaras, C. V.; Durst, H. D. Evaporation and degradation of VX on silica sand. *J. Phys. Chem. C* **2009**, *113*, 6622−6633.

DOI: 10.1021/acs.iecr.9b01270
Ind. Eng. Chem. Res. 2019, 58, 10383−10393

(35) Wagner, G. W.; Procell, L. R.; O'Connor, R. J.; Munavalli, S.; Carnes, C. L.; Kapoor, P. N.; Klabunde, K. J. Reactions of VX, GB, GD, and HD with nanosize Al_2O_3. Formation of aluminophosphonates. *J. Am. Chem. Soc.* **2001**, *123*, 1636−1644.
(36) Columbus, I.; Waysbort, D.; Shmueli, L.; Nir, I.; Kaplan, D. Decomposition of adsorbed VX on activated carbons studied by ^{31}P MAS NMR. *Environ. Sci. Technol.* **2006**, *40*, 3952−3958.
(37) Mizrahi, D. M.; Columbus, I. ^{31}P MAS NMR: A useful tool for the evaluation of VX natural weathering in various urban matrixes. *Environ. Sci. Technol.* **2005**, *39*, 8931−8935.
(38) Wagner, G. W.; Fry, R. A. Observation of distinct surface Al_{IV} sites and phosphonate binding modes in γ-alumina and concrete by high-field ^{27}Al and ^{31}P MAS NMR. *J. Phys. Chem. C* **2009**, *113*, 13352−13357.
(39) Kollo, M.; Kudrjasova, M.; Kulp, M.; Aav, R. Methylphosphonic acid as a ^{31}P-NMR standard for the quantitative determination of phosphorus in carbonated beverages. *Anal. Methods* **2013**, *5*, 4005−4009.
(40) Rothwell, W. P.; Waugh, J. S.; Yesinowski, J. P. High-resolution variable-temperature ^{31}P NMR of solid calcium phosphates. *J. Am. Chem. Soc.* **1980**, *102*, 2637−2643.
(41) MacKenzie, K.J.D.; Smith, M.E. *Multinuclear Solid-State NMR of Inorganic Materials*; Elsevier Science: Oxford, UK, 2002.
(42) Wagner, G. W.; MacIver, B. K. Degradation and fate of mustard in soil as determined by ^{13}C MAS NMR. *Langmuir* **1998**, *14*, 6930−6934.

DOI: 10.1021/acs.iecr.9b01270
Ind. Eng. Chem. Res. 2019, 58, 10383−10393